MOX-Report No. 44/2016

A Mixed Finite Element Method for Modeling the Fluid Exchange between Microcirculation and Tissue Interstitium

Notaro, D.; Cattaneo, L.; Formaggia, L.; Scotti, A.; Zunino, P.

MOX, Dipartimento di Matematica
Politecnico di Milano, Via Bonardi 9 - 20133 Milano (Italy)

mox-dmat@polimi.it http://mox.polimi.it

A Mixed Finite Element Method for Modeling the Fluid Exchange between Microcirculation and Tissue Interstitium

Domenico Notaro, Laura Cattaneo, Luca Formaggia, Anna Scotti and Paolo Zunino

Abstract Thanks to dimensional (or topological) model reduction techniques, small inclusions in a three-dimensional (3D) continuum can be described as one-dimensional (1D) concentrated sources, in order to reduce the computational cost of simulations. However, concentrated sources lead to singular solutions that still require computationally expensive graded meshes to guarantee accurate approximation. The main computational barrier consists in the ill-posedness of restriction operators (such as the trace operator) applied on manifolds with co-dimension larger than one. We overcome the computational challenges of approximating PDEs on manifolds with high dimensionality gap by means of nonlocal restriction operators that combine standard traces with mean values of the solution on low dimensional manifolds. This new approach has the fundamental advantage of enabling the approximation of the problem using Galerkin projections on Hilbert spaces, which could not be otherwise applied because of regularity issues. This approach, previously applied to second order PDEs, is extended here to the mixed formulation of flow problems with applications to microcirculation. In this way we calculate, in the bulk and on the 1D manifold simultaneously, the approximation of velocity and pressure fields that guarantees good accuracy with respect to mass conservation.

1 Introduction

The ultimate objective of the project is to perform large scale simulations of microcirculation. In the context of blood flow, the application of geometrical model reduction techniques plays an essential role, see for example [10, 18]. In particular, small vessels embedded into a continuum can be described as one-dimensional

Domenico Notaro, Laura Cattaneo, Luca Formaggia, Anna Scotti and Paolo Zunino
MOX, Department of Mathematics, Politecnico di Milano, piazza Leonardo da Vinci 32, 20133 Milano, e-mail: domenico.notaro@mail.polimi.it, laura1.cattaneo@polimi.it, luca.formaggia@polimi.it, anna.scotti@polimi.it, paolo.zunino@polimi.it

(1D) concentrated sources, in order to reduce the computational cost of simulations. Although the coupling of three-dimensional (3D) continua with embedded (1D) networks arises in applications of paramount importance such as microcirculation, flow through perforated media and the study of reinforced materials, it has not been well investigated yet.

Two remarkable examples of methods that were previously proposed to overcome the challenges of simulating small objects into a continuum are the *immersed boundary methods* [15, 17, 22] and the *fictitious domain methods* [11, 12, 21]. Although they share some similarities with the approach that we pursue here, they have never been applied for solving coupled partial differential equations on embedded domains.

In the particular case of microcirculation, many ad-hoc approaches have been proposed. Since capillaries can be modelled as long and narrow cylindrical vessels, asymptotic expansions that exploit the large aspect ratio of the channel can be derived to approximate the fluid exchange from one capillary to the surrounding tissue. This idea has been successfully exploited to study the microvascular flow in simple arrays of capillaries [1, 8, 9]. However, vascular networks are characterized by a complex, possibly irregular geometry. The previous semi-analytic methods may be hardly applied to realistic configurations. We believe that numerical methods may override this obstacle. For example, the method of Green's functions, has been extensively applied to the study complex vascular networks of tumors [13, 19, 20].

In this work we aim to move away from ad-hoc approaches and cast the microcirculation problem into a new unified framework to formulate and approximate coupled partial differential equations (PDEs) on manifolds with heterogeneous dimensionality. The main computational barrier consists in the ill-posedness of restriction operators (such as the trace operator) applied on manifolds with co-dimension larger than one. Following the approach introduced in [7, 14, 6], we will overcome the computational challenges of approximating PDEs on manifolds with high dimensionality gap. The main idea consists of introducing nonlocal restriction operators that combine standard traces with mean values of the solution on low dimensional manifolds, in order to couple the problem solution in 3D with the one in 1D. This new approach has the fundamental advantage to enable the approximation of the problem using Galerkin projections on Hilbert spaces, which could not be otherwise applied, because of regularity issues.

Within this general framework, the specific objective of this work is to formulate the microcirculation problem as a system of coupled 1D and 3D partial differential equations governing the flow through the capillary network and the interstitial volume, respectively. In order to obtain a good approximation of pressure and velocity fields, and in particular to satisfy mass conservation, we formulate the problem in mixed form. Then, we derive a discretization method based on mixed finite elements. Before moving forward to address applications of the method to study pathologies related to microcirculation, such as cancer [4, 3, 16], we address here a thorough validation of the solver based on two benchmark problems.

2 Model set up

We study a mathematical model for fluid transport in a permeable biological tissue perfused by a capillary network. The domain where the model is defined is composed by two parts, Ω and Λ, denoting the interstitial volume and the capillary bed respectively. We assume that the capillaries can be described as cylindrical vessels and Λ denotes the centerline of the capillary network. The capillary radius, R, is for simplicity considered to be constant. We decompose the network Λ into individual branches Λ_i. Branches are parametrized by the arc length s_i; a tangent unit vector $\boldsymbol{\lambda}_i$ is also defined over each branch, defining in this way an arbitrary branch orientation. Differentiation over the branches is defined using the tangent unit vector as $\partial_{s_i} := \nabla \cdot \boldsymbol{\lambda}_i$ on Λ_i, i.e. ∂_{s_i} represents the projection of ∇ along λ_i. The blood flow along each branch is described by Poiseuille's law for conservation of momentum and mass:

$$\mathbf{u}_v^i = -\frac{R^2}{8\mu}\frac{\partial p_{v,i}}{\partial s_i}\boldsymbol{\lambda}_i, \quad -\pi R^2 \frac{\partial \mathbf{u}_v^i}{\partial s_i} = g_i \qquad \text{on} \quad \Lambda_i, \tag{1}$$

where g_i is the transmural flux leaving the vessel. As a consequence of the geometrical assumptions, the vessel velocity has fixed direction and unknown scalar component along the branches, namely $\mathbf{u}_v^i = u_v^i \boldsymbol{\lambda}_i$. We shall hence formulate the vessel problem using the scalar unknown u_v. The governing flow equations for the whole network Λ are obtained by summing (1) over the index i.

We consider the interstitial volume Ω as an isotropic porous medium, described by the Darcy's law, namely

$$\mathbf{u}_t = -\frac{1}{\mu}\mathbb{K}\nabla p_t, \tag{2}$$

where $\mathbf{u}_t$ is the average velocity vector in the tissue, $\mathbb{K} = k\mathbb{I}$ is the isotropic permeability tensor, μ is the viscosity of the fluid and p_t is the fluid pressure.

The coupled problem for microcirculation and interstitial flow reads as follows

$$\begin{cases} \dfrac{\mu}{k}\mathbf{u}_t + \nabla p_t = 0 & \text{in} \quad \Omega, \\ \nabla \cdot \mathbf{u}_t - f(p_t, p_v)\delta_\Lambda = 0 & \text{in} \quad \Omega, \\ \dfrac{8\mu}{R^2}u_v + \dfrac{\partial p_v}{\partial s} = 0 & \text{in} \quad \Lambda, \\ \dfrac{\partial u_v}{\partial s} + \dfrac{1}{\pi R^2}f(p_t, p_v) = 0 & \text{in} \quad \Lambda. \end{cases} \tag{3}$$

For brevity, we avoid to number each equation of systems. In the remainder, we will refer to single sub-equations within a system using letters, e.g (3) (a),(b),(c),(d).

The constitutive law for blood leakage from the capillaries to the tissue is provided by means of Starling's law of filtration,

$$f(p_t, p_v) = 2\pi R L_p(p_v - \bar{p}_t), \tag{4}$$

with

$$\bar{p}_t(s) = \frac{1}{2\pi R}\int_0^{2\pi} p_t(s,\theta) R d\theta. \tag{5}$$

Before proceeding, we write the equations in dimensionless form. We choose length, velocity and pressure as primary variables for the analysis. The corresponding characteristic values are: (i) the average spacing between capillary vessels d, (ii) the average velocity in the capillary bed U, and (iii) the average pressure in the interstitial space P. The dimensionless groups affecting our equations are:

- $R' = \dfrac{R}{d}$, non-dimensional radius
- $\kappa_t = \dfrac{k}{\mu}\dfrac{P}{Ud}$, hydraulic conductivity of the tissue
- $Q = 2\pi R' L_p \dfrac{P}{U}$, hydraulic conductivity of the capillary walls
- $\kappa_v = \dfrac{\pi R'^4}{8\mu}\dfrac{Pd}{U}$, hydraulic conductivity of the capillary bed

and the corresponding dimensionless equations read as follows

$$\begin{cases} \dfrac{1}{\kappa_t}\mathbf{u}_t + \nabla p_t = 0 & \text{in} \quad \Omega, \\ \nabla\cdot\mathbf{u}_t - Q\,(p_v - \bar{p}_t)\,\delta_\Lambda = 0 & \text{in} \quad \Omega, \\ \dfrac{\pi R'^2}{\kappa_v} u_v + \dfrac{\partial p_v}{\partial s} = 0 & \text{in} \quad \Lambda, \\ \dfrac{\partial u_v}{\partial s} + \dfrac{1}{\pi R'^2} Q\,(p_v - \bar{p}_t) = 0 & \text{in} \quad \Lambda. \end{cases} \tag{6}$$

For simplicity of notation, we used the same symbols for the dimensionless variables, i.e velocities and pressure scaled by U and P, respectively.

Remark 1. Equations (6.b),(6,d) can be combined up to obtain a more meaningful formulation of the mass conservation law, namely

$$\nabla\cdot\mathbf{u}_t + \pi R'^2 \frac{\partial u_v}{\partial s}\delta_\Lambda = 0 \qquad \text{in} \quad \Omega, \tag{7}$$

meaning that the total amount of fluid in the domain $\Omega\cup\Lambda$ must be preserved.

Boundary conditions will be specified further on for both the tissue and vessel problems. The imposition of suitable compatibility conditions at the bifurcations or branching points of the capillary tree is also necessary to guarantee well posedness of (6). Specifically, we shall enforce conservation of mass and continuity of total pressure at junctions. Let us introduce these conditions in a simple Y-shaped bifurcation network (Fig. 1). Since in the reduced 1D model of the capillary network the cross-section is supposed to be constant over the whole network, the conservation of flow rate is equivalent to require that in correspondence of the junction point $\mathbf{x}_M$ the inflow velocity u_v^0 is equal the sum of the outflow velocities u_v^1, u_v^2, namely

$u_v^0(\mathbf{x}_M) = u_v^1(\mathbf{x}_M) + u_v^2(\mathbf{x}_M)$. Similarly, we require the pressure over each branch to be the same at the junction, namely $p_v^0(\mathbf{x}_M) = p_v^1(\mathbf{x}_M) = p_v^2(\mathbf{x}_M)$. The general case of an arbitrary number of *critical* points, possibly with different number of inflow and outflow branches, will be described in Sec. 3.1. Indeed, it is important to emphasize that such compatibility conditions will be enforced in a natural way, at the level of the variational formulation.

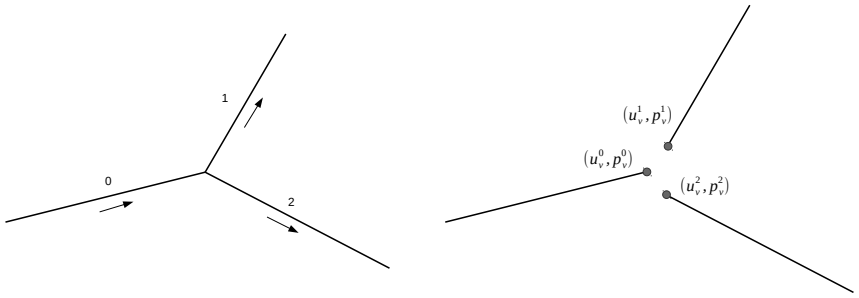

Fig. 1 On the left, a simple network made by a single Y-shaped bifurcation. Arrows show the flow orientation of one inflow branch on the left of the bifurcation point and two outflow branches on the right. On the right, the discretization of vessels network is shown. The domain has been split into branches, the flow problem is defined over each branch and compatibility conditions are enforced at the junction point.

3 Variational formulation

In order to obtain the weak formulation of the tissue interstitium problem, we multiply equations (6) (a,b) with sufficiently smooth functions and integrate over the volume Ω, namely

$$\int_\Omega \frac{1}{\kappa_t}\,\mathbf{u}_t \cdot \mathbf{v}_t \, d\mathbf{x} + \int_\Omega \nabla p_t \cdot \mathbf{v}_t \, d\mathbf{x} = 0, \tag{8}$$

$$\int_\Omega (\nabla \cdot \mathbf{u}_t)\, q_t \, d\mathbf{x} - \int_\Omega Q\,(p_v - \bar{p}_t)\,\delta_\Lambda \, q_t \, d\mathbf{x} = 0. \tag{9}$$

We now apply the Green's theorem to (8) to obtain an anti-symmetric formulation of the Darcy's problem in the tissue:

$$\int_\Omega \frac{1}{\kappa_t}\,\mathbf{u}_t \cdot \mathbf{v}_t \, d\mathbf{x} - \int_\Omega p_t\,(\nabla \cdot \mathbf{v}_t)\, d\mathbf{x} + \int_{\partial\Omega} p_t\,\mathbf{v}_t \cdot \mathbf{n}\, d\sigma(\mathbf{x}) = 0, \tag{10}$$

$$\int_\Omega (\nabla \cdot \mathbf{u}_t)\, q_t \, d\mathbf{x} - \int_\Omega Q\,(p_v - \bar{p}_t)\,\delta_\Lambda \, q_t \, d\mathbf{x} = 0. \tag{11}$$

As concerns the choice of boundary conditions, for simplicity, we enforce a given pressure distribution over $\partial\Omega$, namely

$$p_t = g_t \quad \text{on} \quad \partial\Omega, \tag{12}$$

where $g_t \in L^2(\partial\Omega)$. The weak formulation of the problem in Ω reads

$$\int_\Omega \frac{1}{\kappa_t}\mathbf{u}_t \cdot \mathbf{v}_t \, d\mathbf{x} - \int_\Omega p_t \, (\nabla \cdot \mathbf{v}_t) \, d\mathbf{x} = -\int_{\partial\Omega} g_t \, \mathbf{v}_t \cdot \mathbf{n} \, d\sigma(\mathbf{x})$$
$$\int_\Omega (\nabla \cdot \mathbf{u}_t) \, q_t \, d\mathbf{x} - \int_\Omega Q\,(p_v - \bar{p}_t)\,\delta_\Lambda \, q_t \, d\mathbf{x} = 0 \quad .$$

For the vessel problem we start giving a general functional framework. At this point, we only require regularity for vessel velocity and pressure over each branch separately:

$$V_v = \bigcup_{i=1}^{N} H^1(\Lambda_i) \qquad Q_v = \bigcup_{i=1}^{N} L^2(\Lambda_i).$$

The definition of trial and test spaces will be revised in the sequel, in the light of the particular junction conditions we will chose, while no boundary conditions are enforced in the definition of the spaces. As for the tissue problem, we multiply equations (6.c),(6.d) by sufficiently smooth test functions and integrate over Λ:

$$\int_\Lambda \frac{\pi R'^2}{\kappa_v} u_v \, v_v \, ds + \int_\Lambda \frac{\partial p_v}{\partial s} \, v_v \, ds = 0, \tag{13}$$

$$\int_\Lambda \frac{\partial u_v}{\partial s} \, q_v \, ds + \frac{1}{\pi R'^2} \int_\Lambda Q\,(p_v - \bar{p}_t) \, q_v \, ds = 0. \tag{14}$$

The integration by parts is not trivial in this case because the vessel variables p_v and u_v *may* be discontinuous at multiple junctions. Let us treat separately the second integral of (13) and decompose it over the individual branches Λ_i:

$$\int_\Lambda \frac{\partial p_v}{\partial s} \, v_v \, ds = \sum_{i=1}^{N} \int_{\Lambda_i} \frac{\partial p_v}{\partial s} \, v_v \, ds = -\int_\Lambda p_v \frac{\partial v_v}{\partial s} \, ds + \sum_{i=1}^{N} [\, p_v \, v_v \,]_{\Lambda_i^-}^{\Lambda_i^+}, \tag{15}$$

where Λ_i^- and Λ_i^+ represent the inflow and outflow boundaries of Λ_i, according to the orientation $\boldsymbol{\lambda}_i$. Let us define the set of the indexes of junction points:

$$\mathscr{J} := \left\{ \; j \in \mathbb{N} \; : \; s_j \in \Lambda, \, \#(P_{s_j}) \geq 2 \; \right\},$$

where P_{s_j} is the *patch* of the j-th junction node, i.e. the collection of all branches joining at the node, and # indicates the counting measure. We also need the following disjoint partition of the indexes in P_{s_j}. According to the orientation unit vector $\boldsymbol{\lambda}_i$, for any branching point s_j we distinguish branches that are entering the node, whose contribution to mass conservation is positive, from branches who are leaving

the node, whose contribution is negative. The former are branches whose outflow region coincides with the point s_j, while for the latter it is the inflow region:

$$\mathscr{P}_j^{out} := \left\{ i \in \{1,\dots,N\} \,:\, \Lambda_i^+ \equiv \{s_j\} \right\},$$
$$\mathscr{P}_j^{in} := \left\{ i \in \{1,\dots,N\} \,:\, \Lambda_i^- \equiv \{s_j\} \right\},$$

for all $j \in \mathscr{J}$. At this point, the fluid mass conservation at each node can be expressed as follows

$$\sum_{i \in \mathscr{P}_j^{out}} u_v|_{\Lambda_i^+} - \sum_{i \in \mathscr{P}_j^{in}} u_v|_{\Lambda_i^-} = 0, \quad \forall j \in \mathscr{J}, \tag{16}$$

where $\Lambda^{in}, \Lambda^{out}$ indicate the collection of inflow and outflow boundaries of the vessel network, i.e. non junction points where the tangent unit vector is inward-pointing and outward-pointing, respectively. This collection contains the boundary points, i.e. the extrema that also belong to $\partial\Omega$, but the inclusion may be strict. However, in this contribution we do not address the issue of network extrema belonging to $\mathring{\Omega}$, i.e. we do not consider immersed tips.

In order to enforce such conditions, we proceed as follows. First, we reformulate the last term in (15) by isolating the terms relative to inflow junction nodes from those relative to outflow nodes, namely

$$\sum_{i=1}^{N} [p_v v_v]_{\Lambda_i^-}^{\Lambda_i^+} = \sum_{j \in \mathscr{J}} \left[\sum_{i \in \mathscr{P}_j^{out}} p_v v_v|_{\Lambda_i^+} - \sum_{i \in \mathscr{P}_j^{in}} p_v v_v|_{\Lambda_i^-} \right] + [p_v v_v]_{\Lambda^{in}}^{\Lambda^{out}}.$$

Here, we have implicitly assumed the trace of $(p_v v_v)$ over Λ_i exists for v_v smooth enough, i.e. the evaluation of the product at the extrema of Λ_i makes sense. Furthermore, we write $(p_v v_v)(s_j) = p_v(s_j)\, v_v(s_j)$ for some point $s_j \in \Lambda$. This is feasible if the trace of the pressure exists. Obviously, a general L^2 function is not sufficient, the natural choice is $p_v \in \mathscr{C}^0(\bar{\Lambda})$, that in particular implies compatibility of pressure values at the junctions. Indeed, if the pressure is continuous at the junction, we have

$$p_v|_{\Lambda_i^-} \equiv p_v(s_j) \equiv p_v|_{\Lambda_k^+} \quad \forall i \in \mathscr{P}_j^{in},\, k \in \mathscr{P}_j^{out} \quad \forall j \in \mathscr{J}. \tag{17}$$

Under that hypothesis, we finally factorize out the pressure and isolate a term that corresponds to the junction conditions for the velocity test functions, that is

$$\sum_{j \in \mathscr{J}} p_v(s_j) \left[\sum_{i \in \mathscr{P}_j^{out}} v_v|_{\Lambda_i^+} - \sum_{i \in \mathscr{P}_j^{in}} v_v|_{\Lambda_i^-} \right].$$

Then, we weakly enforce mass conservation into the variational formulation by multiplying (16) by the pressure test functions q_v, which act as a Lagrange multiplier

for this constraint, namely

$$\sum_{j\in\mathscr{J}} q_v(s_j)\left[\sum_{i\in\mathscr{P}_j^{out}} u_v|_{\Lambda_i^+} - \sum_{i\in\mathscr{P}_j^{in}} u_v|_{\Lambda_i^-}\right].$$

Finally, after adding the previous term to equation (14), the weak formulation of the vessel problem reads

$$\begin{aligned}\int_\Lambda \frac{\pi R'^2}{\kappa_v}\, u_v\, v_v\, ds \;-\; \int_\Lambda p_v \frac{\partial v_v}{\partial s}\, ds \;+\; [p_v\, v_v]_{\Lambda^{in}}^{\Lambda^{out}} \\ +\; \sum_{j\in\mathscr{J}} p_v(s_j)\left[\sum_{i\in\mathscr{P}_j^{out}} v_v|_{\Lambda_i^+} - \sum_{i\in\mathscr{P}_j^{in}} v_v|_{\Lambda_i^-}\right] \;=\; 0,\end{aligned} \tag{18}$$

$$\begin{aligned}\int_\Lambda \frac{\partial u_v}{\partial s}\, q_v\, ds \;+\; \frac{1}{\pi R'^2}\int_\Lambda Q\,(p_v-\bar{p}_t)\, q_v\, ds \\ -\; \sum_{j\in\mathscr{J}} q_v(s_j)\left[\sum_{i\in\mathscr{P}_j^{out}} u_v|_{\Lambda_i^+} - \sum_{i\in\mathscr{P}_j^{in}} u_v|_{\Lambda_i^-}\right] \;=\; 0.\end{aligned} \tag{19}$$

Concerning the boundary conditions for the vessels network, the natural choice is to enforce a given pressure distributions at the inflow and the outflow of the network, $p_v = g_v$ on $\Lambda^{in}\cup\Lambda^{out}$. The generic regularity requirements for the Dirichlet's datum are measurability and square-summability, namely $g_v \in L^2(\Lambda^{in}\cup\Lambda^{out})$. In practice, we consider a constant pressure drop $\Delta P_v = P_v^{out} - P_v^{in}$:

$$g_v(s) = \begin{cases} P_v^{in} & s\in\Lambda^{in} \\ P_v^{out} & s\in\Lambda^{out}. \end{cases} \tag{20}$$

Since we are considering the mixed formulation of the problem, we enforce such condition in a weak *natural* way.

At this point, we combine (10), (11), (18), (19) to obtain the whole weak formulation of our 3D-1D coupled model of fluid exchange between microcirculation and tissue interstitium. The variational formulation of problem (6) consists of finding $\mathbf{u}_t \in \mathbf{V}_t$, $p_t \in Q_t$, $u_v \in V_v$, $p_v \in Q_v$ s.t.

$$
\begin{cases}
\dfrac{1}{\kappa_t}\big(\mathbf{u}_t\,,\mathbf{v}_t\big)_\Omega \;-\; \big(p_t\,,\nabla\cdot\mathbf{v}_t\big)_\Omega \;=\; -\;\big(g_t\,,\mathbf{v}_t\cdot\mathbf{n}\big)_{\partial\Omega} & \forall \mathbf{v}_t\in\mathbf{V}_t,\\[2ex]
\big(\nabla\cdot\mathbf{u}_t\,,q_t\big)_\Omega \;-\; Q\big(\,(p_v-\bar p_t)\,\delta_\Lambda\,,q_t\big)_\Omega \;=\; 0 & \forall q_t\in Q_t,\\[2ex]
\dfrac{\pi R'^2}{\kappa_v}\big(u_v\,,v_v\big)_\Lambda \;-\; \big(p_v\,,\partial_s v_v\big)_\Lambda & \\
\qquad +\;\sum_j p_v(s_j)\Big[\sum_i v_v|_{\Lambda_i^+}-\sum_i v_v|_{\Lambda_i^-}\Big] \;=\; -\,[g_v\,v_v]_{\Lambda\,in}^{\Lambda\,out} & \forall v_v\in V_v,\\[2ex]
\big(\partial_s u_v\,,q_v\big)_\Lambda \;+\; \dfrac{1}{\pi R'^2}\,Q\big(p_v-\bar p_t\,,q_v\big)_\Lambda & \\
\qquad -\;\sum_j q_v(s_j)\Big[\sum_i u_v|_{\Lambda_i^+}\;-\;\sum_i u_v|_{\Lambda_i^-}\Big] \;=\; 0 & \forall q_v\in Q_v.
\end{cases}
\tag{21}
$$

4 Numerical approximation

The discretization of problem (6) is achieved by means of the finite element method that arises from the variational formulation (21) combined with a discretization of the domain. In particular, one of the advantage of our formulation is that the partitions of Ω and Λ are completely independent. Let us now analyze the two approximations separately.

We denote with $\mathscr{T}_t^h$ an admissible family of partitions of $\bar\Omega$ into tetrahedrons K

$$\bar\Omega = \bigcup_{K\in\mathscr{T}_t^h} K,$$

that satisfies the usual conditions of a conforming triangulation of Ω. Here, h denotes the mesh characteristic size, i.e. $h=\max_{K\in\mathscr{T}_t^h} k_K$, being h_K the diameter of simplex K. Moreover, we are implicitly assuming that Ω is a *polygonal* domain. The solutions of (21)(a,b) are approximated using discontinuous piecewise-polynomial finite elements for pressure and $\mathbf{H}^{div}$-conforming *Raviart-Thomas* finite elements [2] for velocity, namely

$$
\begin{aligned}
\mathbb{Y}_h^k &:= \big\{\; w_h\in L^2(\Omega)\;:\; w_h|_K\in\mathscr{P}_{k-1}(K)\quad\forall K\in\mathscr{T}_t^h\;\big\},\\
\mathbb{RT}_h^k &:= \big\{\; \mathbf{w}_h\in\mathbf{H}((div,\Omega)\;:\; \mathbf{w}_h|_K\in\mathscr{P}_{k-1}(K;\mathbb{R}^d)\oplus\mathbf{x}\,\mathscr{P}_{k-1}(K)\quad\forall K\in\mathscr{T}_t^h\;\big\},
\end{aligned}
$$

for every integer $k\geq 0$, where $\mathscr{P}_k$ indicates the standard space of polynomials of degree $\leq k$ in the variables $\mathbf{x}=(x_1,\ldots,x_d)$. For the simulations presented later on, the lowest order *Raviart-Thomas* approximation has been adopted, corresponding to $k=1$ above. In numerical experiments performed on the 3D problem alone (the test case is not reported here), we have observed quadratic convergence of the pressure field and linear convergence of the velocity field.

Concerning the capillary network, we adopt the same domain splitting technique described at the continuous level, obtaining the following discrete domain:

$$\Lambda_h = \bigcup_{i=1}^{N} \Lambda_i^h,$$

where Λ_i^h is a finite element mesh on the one-dimensional manifold Λ_i, i.e. a partition of the i-th network branch made by a sufficiently large number of segments. The solution of sub-equations (21c), (21d) over a given branch Λ_i is approximated using continuous piecewise-polynomial finite element spaces for both pressure and velocity. Since we want the vessel velocity to be discontinuous at multiple junctions, we define the related finite element space over the whole network as the collection of the local spaces of the single branches. Conversely, the pressure has been assumed to be continuous over the network. We will use the following families of finite element spaces for pressure and velocity, respectively:

$$\begin{aligned}
\mathbb{X}_h^{k+1}(\Lambda) &:= \left\{ w_h \in \mathscr{C}^0(\bar{\Lambda}) \ : \ w_h|_S \in \mathscr{P}_k(S) \quad \forall S \in \Lambda^h \right\}, \\
\mathbb{W}_h^{k+2}(\Lambda) &:= \bigcup_{i=1}^{N} \mathbb{X}_h^{k+1}(\Lambda_i),
\end{aligned}$$

for every integer $k \geq 0$. As a result, we use generalized Taylor-Hood elements on each network branch, satisfying in this way the local stability of the mixed finite element pair for the network. At the same time, we guarantee that the pressure approximation is continuous over the entire network Λ. In particular, for the numerical experiments shown later on we have used the lowest order, that is $k = 1$.

The discrete formulation arising from (21) is hence easily obtained by adding the subscript h to the weak continuous formulation: find $\mathbf{u}_{t,h} \in \mathbf{V}_t^h$, $p_{t,h} \in Q_t^h$, $u_{v,h} \in V_v^h$, $p_{v,h} \in Q_v^h$ s.t.

$$\begin{cases}
\dfrac{1}{\kappa_t}\left(\mathbf{u}_{t,h}, \mathbf{v}_{t,h}\right)_\Omega - \left(p_{t,h}, \nabla\cdot\mathbf{v}_{t,h}\right)_\Omega = -\left(g_{t,h}, \mathbf{v}_{t,h}\cdot\mathbf{n}\right)_{\partial\Omega} & \forall \mathbf{v}_{t,h} \in \mathbf{V}_t^h, \\
\left(\nabla\cdot\mathbf{u}_{t,h}, q_{t,h}\right)_\Omega - Q\left(\left(p_{v,h} - \bar{p}_{t,h}\right)\delta_\Lambda, q_{t,h}\right)_\Omega = 0 & \forall q_{t,h} \in Q_t^h, \\
\dfrac{\pi R'^2}{\kappa_v}\left(u_{v,h}, v_{v,h}\right)_\Lambda - \left(p_{v,h}, \partial_s v_{v,h}\right)_\Lambda & \\
\quad + \sum_j p_{v,h}(s_j)\left[\sum_i v_{v,h}|_{\Lambda_i^+} - \sum_i v_{v,h}|_{\Lambda_i^-}\right] = -\left[g_{v,h}\, v_{v,h}\right]_{\Lambda^{in}}^{\Lambda^{out}} & \forall v_{v,h} \in V_v^h \\
\left(\partial_s u_{v,h}, q_{v,h}\right)_\Lambda + \dfrac{1}{\pi R'^2} Q\left(p_{v,h} - \bar{p}_{t,h}, q_{v,h}\right)_\Lambda & \\
\quad - \sum_j q_{v,h}(s_j)\left[\sum_i u_{v,h}|_{\Lambda_i^+} - \sum_i u_{v,h}|_{\Lambda_i^-}\right] = 0 & \forall q_{v,h} \in Q_v^h,
\end{cases} \tag{22}$$

where $g_{t,h}$, $g_{v,h}$ indicate the discrete counterparts of continuous boundary data.

We observe that (22) is a generalized saddle-point problem arising from the combination of local problems with mass conservation constraints (see also (23)), such as the mixed formulation of Darcy equation and the incompressible flow on each

network branch with junction conditions. Although, we guarantee local stability of each block, the global well-posedness is an still an open problem, which is under investigation.

4.1 Algebraic formulation

Let us now derive the algebraic form of our discrete problem. We define the number of degrees of freedom of our discrete (finite) spaces as:

$$N_t^h := dim\left(\mathbf{V}_t^h\right), \qquad M_t^h := dim\left(Q_t^h\right),$$
$$N_v^h := dim\left(V_v^h\right), \qquad M_v^h := dim\left(Q_v^h\right) \quad .$$

We denote with $\{\boldsymbol{\varphi}_t^i\}_{i=1}^{N_t^h} \times \{\psi_t^i\}_{i=1}^{M_t^h}$ and $\{\boldsymbol{\varphi}_v^i\}_{i=1}^{N_v^h} \times \{\psi_v^i\}_{i=1}^{M_v^h}$ the finite element basis for $\mathbf{V}_t^h \times Q_t^h$ and $V_v^h \times Q_v^h$ respectively. These two sets are completely independent, since the 3D and 1D meshes do not conform. We set:

$$\mathbf{u}_t^h(\mathbf{x}) = \sum_{j=1}^{N_t^h} U_t^j \ \boldsymbol{\varphi}_t^j(\mathbf{x}), \quad p_t^h(\mathbf{x}) = \sum_{j=1}^{M_t^h} P_t^j \ \psi_t^j(\mathbf{x}) \qquad \forall \mathbf{x} \in \Omega_t,$$
$$u_v^h(s) = \sum_{j=1}^{N_v^h} U_v^j \ \varphi_v^j(s), \quad p_v^h(s) = \sum_{j=1}^{M_v^h} P_v^j \ \psi_v^j(s) \qquad \forall s \in \Lambda,$$

being $\mathbf{U}_t = \{U_t^j\}_{j=1}^{N_t^h}$, $\mathbf{P}_t = \{P_t^j\}_{j=1}^{M_t^h}$, $\mathbf{U}_v = \{U_v^j\}_{j=1}^{N_v^h}$ and $\mathbf{P}_v = \{P_v^j\}_{j=1}^{M_v^h}$, the degrees of freedom of the finite element approximation. Then, by replacing the linear combinations within the discrete weak form (22) and using the linearity of the inner product, from (22) we deduce the following linear system:

$$\begin{bmatrix} \mathbb{M}_{tt} & -\mathbb{D}_{tt}^T & \mathbb{O} & \mathbb{O} \\ \mathbb{D}_{tt} & \mathbb{B}_{tt} & \mathbb{O} & -\mathbb{B}_{tv} \\ \mathbb{O} & \mathbb{O} & \mathbb{M}_{vv} & -\mathbb{D}_{vv}^T - \mathbb{J}_{vv}^T \\ \mathbb{O} & -\mathbb{B}_{vt} & \mathbb{D}_{vv} + \mathbb{J}_{vv} & \mathbb{B}_{vv} \end{bmatrix} \begin{bmatrix} \mathbf{U}_t \\ \mathbf{P}_t \\ \mathbf{U}_v \\ \mathbf{P}_v \end{bmatrix} = \begin{bmatrix} \mathbf{F}_t \\ \mathbf{0} \\ \mathbf{F}_v \\ \mathbf{0} \end{bmatrix}. \tag{23}$$

Standard finite element matrices and right hand sides are defined as follows

$$
\begin{aligned}
&[\mathbb{M}_{tt}]_{i,j} := \frac{1}{\kappa_t}\left(\boldsymbol{\varphi}_t^j, \boldsymbol{\varphi}_t^i\right)_\Omega && \mathbb{M}_{tt} \in \mathbb{R}^{N_t^h \times N_t^h},\\
&[\mathbb{D}_{tt}]_{i,j} := \left(\nabla\cdot\boldsymbol{\varphi}_t^j, \psi_t^i\right)_\Omega && \mathbb{D}_{tt} \in \mathbb{R}^{N_t^h \times M_t^h},\\
&[\mathbb{D}_{vv}]_{i,j} := \left(\partial_s\varphi_v^j, \psi_v^i\right)_\Lambda && \mathbb{D}_{vv} \in \mathbb{R}^{N_v^h \times M_v^h},\\
&[\mathbb{M}_{vv}]_{i,j} := \pi R'^2/\kappa_v\left(\varphi_v^j, \varphi_v^i\right)_\Lambda && \mathbb{M}_{vv} \in \mathbb{R}^{N_v^h \times N_v^h},\\
&[\mathbf{F}_t]_i := -\left(g_{t,h}, \boldsymbol{\varphi}_t^i\cdot\boldsymbol{n}\right)_{\partial\Omega} && \mathbf{F}_t \in \mathbb{R}^{N_t^h},\\
&[\mathbf{F}_v]_i := -[g_{v,h}\,\varphi_v^i]_{\Lambda^{in}}^{\Lambda^{out}} && \mathbf{F}_v \in \mathbb{R}^{N_v^h}.
\end{aligned}
$$

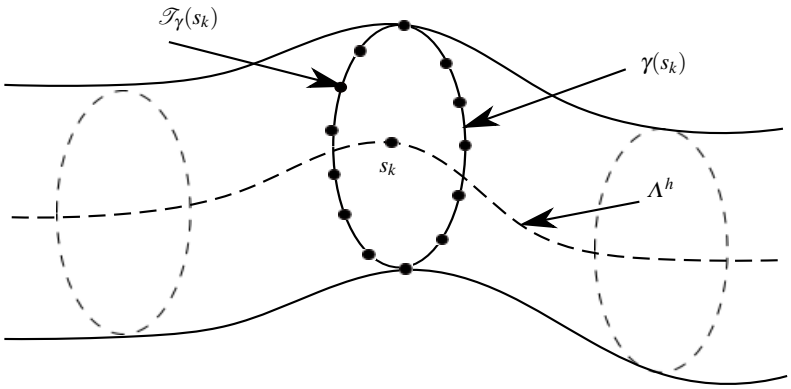

Fig. 2 Illustration of the vessel with its centerline Λ^h, a cross section, its perimeter $\gamma(s_k)$ and its discretization $\mathscr{T}_\gamma(s_k)$ used for the definition of the interface operators $\bar{\pi}_{vt} : Q_t^h \longrightarrow Q_v^h$ and $\pi_{tv} : Q_v^h \longrightarrow Q_t^h$.

For the implementation of exchange matrices, namely $\mathbb{B}_{tt}, \mathbb{B}_{tv}, \mathbb{B}_{vt}, \mathbb{B}_{vv}$, we define two discrete operators: the first one extracts the mean value of a generic basis function of Q_t^h, while the second interpolates between Q_t^h and Q_v^h. For every node $s_k \in \Lambda^h$ we define $\mathscr{T}_\gamma(s_k)$ as the discretization of the perimeter of the vessel $\gamma(s_k)$, see Figure 2 for an illustration. For simplicity, we assume that $\gamma(s_k)$ is a circle of radius R defined on the orthogonal plane to Λ^h at point s_k. The set of points of $\mathscr{T}_\gamma(s_k)$ is used to interpolate the basis functions ψ_t^i. Let us introduce a local discrete interpolation matrix $\Pi_\gamma(s_k)$ which returns the values of each test function ψ_t^i on the set of points belonging to $\mathscr{T}_\gamma(s_k)$. Then, we consider the average operator $\bar{\pi}_{vt} : Q_t^h \longrightarrow Q_v^h$ such that $\bar{q}_t = \bar{\pi}_{vt} q_t$. The matrix $\bar{\Pi}_{vt}$ that corresponds to this operator belongs to $\mathbb{R}^{M_v^h \times M_t^h}$ and it is constructed such that each row is defined as,

$$
\bar{\Pi}_{vt}|_k = \mathbf{w}^T(s_k)\,\Pi_\gamma(s_k) \qquad k = 1, \ldots, M_v^h \tag{24}
$$

where $\mathbf{w}$ are the weights of the quadrature formula used to approximate the integral

$$\bar{q}_t(s) = \frac{1}{2\pi R} \int_0^{2\pi} q_t(s,\theta)\, R\, d\theta$$

on the nodes belonging to $\mathscr{T}_\gamma(s_k)$. The discrete interpolation operator $\pi_{tv} : Q_v^h \longrightarrow Q_t^h$ returns the value of each basis function belonging to Q_t^h in correspondence of nodes of Q_v^h. In algebraic form it is expressed as an interpolation matrix $\Pi_{tv} \in \mathbb{R}^{M_v^h \times M_t^h}$. Using these tools we obtain:

$$\mathbb{B}_{tt} = Q\, \Pi_{vt}^T\, \mathbb{M}_{vv}^P\, \bar{\Pi}_{vt}, \tag{25}$$

$$\mathbb{B}_{tv} = Q\, \Pi_{vt}^T\, \mathbb{M}_{vv}^P, \tag{26}$$

$$\mathbb{B}_{vt} = Q/\pi R'^2\, \mathbb{M}_{vv}^P\, \bar{\Pi}_{vt}, \tag{27}$$

$$\mathbb{B}_{vv} = Q/\pi R'^2\, \mathbb{M}_{vv}^P, \tag{28}$$

being $\mathbb{M}_{vv}^P$ the pressure mass matrix for the vessel problem defined by

$$\left[\mathbb{M}_{vv}^P\right]_{i,j} := \left(\, \psi_v^j\,,\, \psi_v^i \,\right)_\Lambda .$$

Concerning the implementation of junction compatibility conditions, we introduce a linear operator giving the restriction with sign of a basis function of V_v^h over a given junction node. For a given $k \in \mathscr{J}$, we define $\mathscr{R}_k : V_v^h \longrightarrow \mathbb{R}$ such that:

$$\mathscr{R}_k(\,\varphi_v^j\,) := \begin{cases} +\varphi_v^j(s_k) & j\ in\ \Lambda_l^h\ \wedge\ l \in \mathscr{P}_k^{out} \\ -\varphi_v^j(s_k) & j\ in\ \Lambda_l^h\ \wedge\ l \in \mathscr{P}_k^{in} \end{cases} \tag{29}$$

for all $j = 1, \ldots, N_v^h$, where the expression "$j\ in\ \Lambda_l^h$" means that the j-th dof is linked to some vertex of the l-th branch. Note that we are implicitly using the usual property of Lagrangian finite element basis functions, i.e. that they vanish on all nodes except the related one. As a consequence, our definition is consistent for all junction vertexes. Indeed, $\mathscr{R}_k$ may only assume values $-1, 0, +1$ and in particular $\mathscr{R}_k(\,\varphi_v^j\,) = 0$ for all couples of indexes (k, j) that are uncorrelated. Furthermore, the definition of $\mathscr{R}_k$ can be trivially extended to all network vertexes. Using this operator, the generic (i, j) element of $\mathbb{J}_{vv}$ may be computed as follows

$$[\mathbb{J}_{vv}]_{i,j} = -\sum_{k \in \mathscr{J}} \mathscr{R}_k(\,\varphi_v^j\,)\ \psi_v^i(s_k)\,. \tag{30}$$

5 Numerical experiments

We validate the mixed-finite element solver through the following test cases, illustrated in Figure 3, which have been designed to obtain sufficient generality with a straightforward interpretation of the results:

I. Coupled 3D-1D problem on a single branch;

II. Coupled 3D-1D problem on a Y-shaped bifurcation.

In this way, we address the two main modeling issues: (i) first, we test the ability of the computational model to approximate the coupling between 3D and 1D equations; (ii) second, we verify that the assembly of junction conditions works properly.

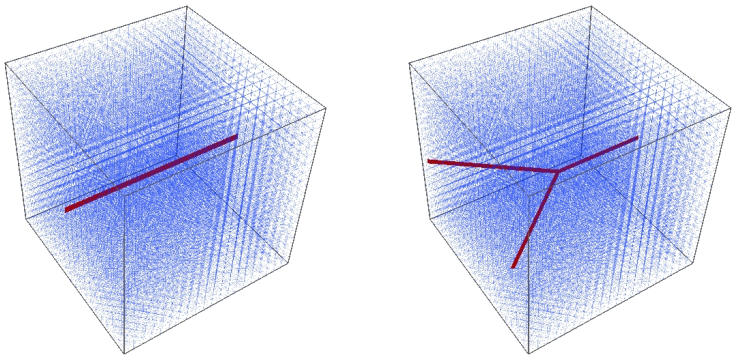

Fig. 3 (left) Computational domain for test-case I. The discrete network Λ_h is made by a single capillary vessel immersed in a unitary slab of tissue interstitium, Ω_h. We have used a discretization step $h = 0.05$ for both the 1D and 3D problems. (right) Computational domain for test-case II. The discrete vessels network Λ_h is made by three capillaries joined junction point $\mathbf{x}_M = (0.5, 0.5, 0.5)$: Λ_h^0 entering branch, Λ_h^1 and Λ_h^2 exiting branches. The tissue interstitium domain Ω_h is a unit cube. Again, we have used a discretization step $h = 0.05$ for both the 1D and 3D problems.

5.1 Coupled 3D-1D problem on a single branch

For such a simple setting, we can easily isolate the exchange terms. The 3D-1D coupled problem is given by (6). In this case, the integration by parts in (6)(iii) is standard since there are not any junction points. As a consequence, we replace condition (15) with the following:

$$\begin{aligned}\int_\Lambda \frac{\partial p_v}{\partial s} v_v \, ds &= -\int_\Lambda p_v \frac{\partial v_v}{\partial s} \, ds + [p_v v_v]_{\Lambda^{in}}^{\Lambda^{out}} \\ &= -\int_0^1 p_v \frac{\partial v_v}{\partial s} \, ds + p_v(1) v_v(1) - p_v(0) v_v(0) \quad .\end{aligned}$$

Therefore, we obtain the following linear system:

$$\begin{bmatrix} \mathbb{M}_{tt} & -\mathbb{D}_{tt}^T & \mathbb{O} & \mathbb{O} \\ \mathbb{D}_{tt} & \mathbb{B}_{tt} & \mathbb{O} & -\mathbb{B}_{tv} \\ \mathbb{O} & \mathbb{O} & \mathbb{M}_{vv} & -\mathbb{D}_{vv}^T \\ \mathbb{O} & -\mathbb{B}_{vt} & \mathbb{D}_{vv} & \mathbb{B}_{vv} \end{bmatrix} \begin{bmatrix} \mathbf{U}_t \\ \mathbf{P}_t \\ \mathbf{U}_v \\ \mathbf{P}_v \end{bmatrix} = \begin{bmatrix} \mathbf{F}_t \\ \mathbf{0} \\ \mathbf{F}_v \\ \mathbf{0} \end{bmatrix} . \tag{31}$$

We recall that submatrices in (31) have been defined in Sec.4.1. Nevertheless, according to the above expression of vessel boundary term it is possible to specify the right hand side, namely

$$\mathbf{F}_v = -[g_{v,h}\,\varphi_v^i]_0^1 \equiv \begin{bmatrix} g_{v,h}(0) \\ 0 \\ \vdots \\ 0 \\ -g_{v,h}(1) \end{bmatrix} \tag{32}$$

being $g_{v,h}$ the discrete counterpart of the vessel boundary datum. In the last equality we used the fundamental property of finite element basis functions. Note that (31) equals the generic linear system (23) in the special case $\mathbb{J}_{vv} = \mathbb{O}$.

5.1.1 Numerical results

For the tissue sample Ω_h we use a tetrahedral structured mesh, $\mathscr{T}_h$, with characteristic size $h = 1/20$; the same step has been used for the network discretization Λ_h, resulting in 48000 elements for the approximation of interstitial volume and 60 elements for the discrete network. We prescribe the following boundary conditions:

$$p_t|_{\partial\Omega} = 0\,, \quad p_v(0) = 1.0\,, \quad p_v(1) = 0.5\,. \tag{33}$$

For the solution of the linear system (31) we developed a C++ code based on GetFEM++ (see https://home.gna.org/getfem), an open-source general purpose finite element library. Specifically, we applied the direct solver *SuperLU* 3.0 (see http://crd.lbl.gov/verb xiaoye/SuperLU). Numerical solutions are shown in Figure 4. These plots show qualitatively that the definition and implementation of the method works properly. In order to find a *quantitative* way to validate our numerical method we exploit the exact solution proposed by J. Chapman and R. Shipley [5] for the single branch problem. In that work the authors model a fluid flow through the leaky neovasculature and porous interstitium of a solid tumor, in particular they consider the simplest case of an isolated capillary immersed in a tumor tissue, giving rise to the the same problem addressed here.

Finally, in order to reproduce numerical results of [5] we choose the non-dimensional parameters of the problem as follows

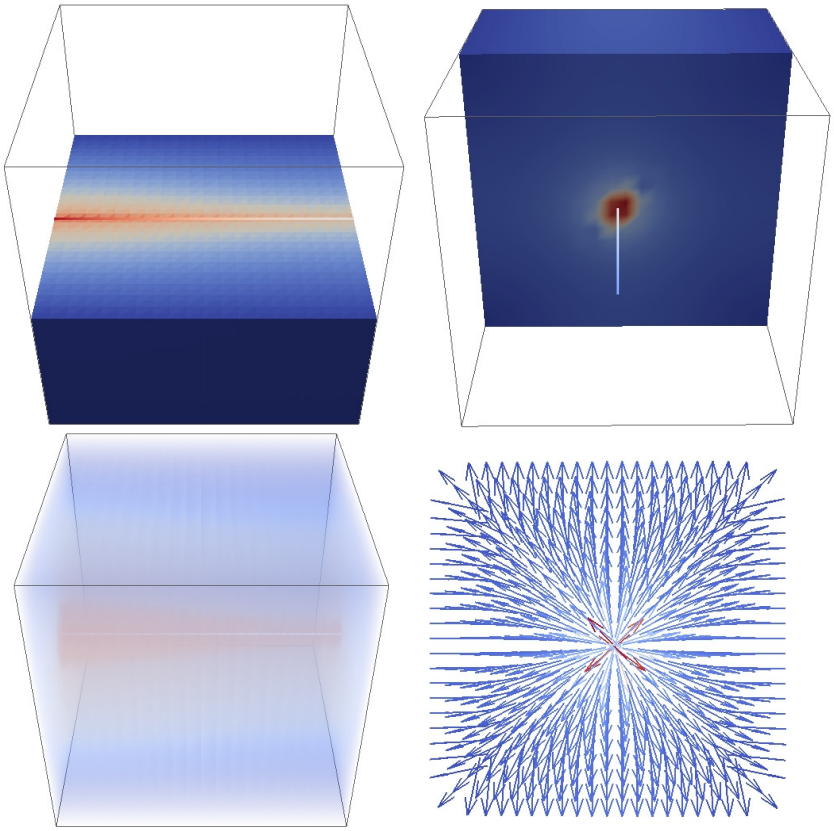

Fig. 4 Coupling between the vessel and tissue interstitium. Numerical solutions obtained with mesh size $h = 0.05$ and parameters $\kappa_t = \kappa_v = 1$, $R' = 1$, $Q = 1$. On the left a double-check for pressure exchange: (top-left) visualization of tissue and vessel pressures at the transversal medium plane, (bottom-left) a 3D qualitative representation. On the right the velocity exchange: (top-right) visualization of tissue and vessel velocities at the axial medium plane, (bottom-right) a 2D view of the vector field.

$$R' = 10^{-2}\,, \quad \kappa_t = 4\,, \quad \kappa_v = \pi R'^3/8\hat{L}_p\,, \quad Q = 2\pi\,, \tag{34}$$

where $\hat{L}_p \in \left\{10^{-4}, 2\times10^{-6}, 10^{-6}, 5\times10^{-7}, 10^{-7}, 10^{-8}\right\}$ is an array of non-dimensional vascular permeabilities used in the numerical tests of [5]. In Figure 5 we represent the capillary pressure as a function of arc-length for different vascular permeabilities. We can observe perfect agreement with the the plots shown in [5] (not reported here). Moreover, we notice that for the lowest value of the vascular permeability $\hat{L}_p$, corresponding to an almost impermeable vessel, the computational model predicts a linearly decreasing pressure, in agreement with the Poiseuille equation that governs the flow. Conversely, for high permeability values there is a substantial deviation from the linear trend because the leakage dominates over the axial flow component.

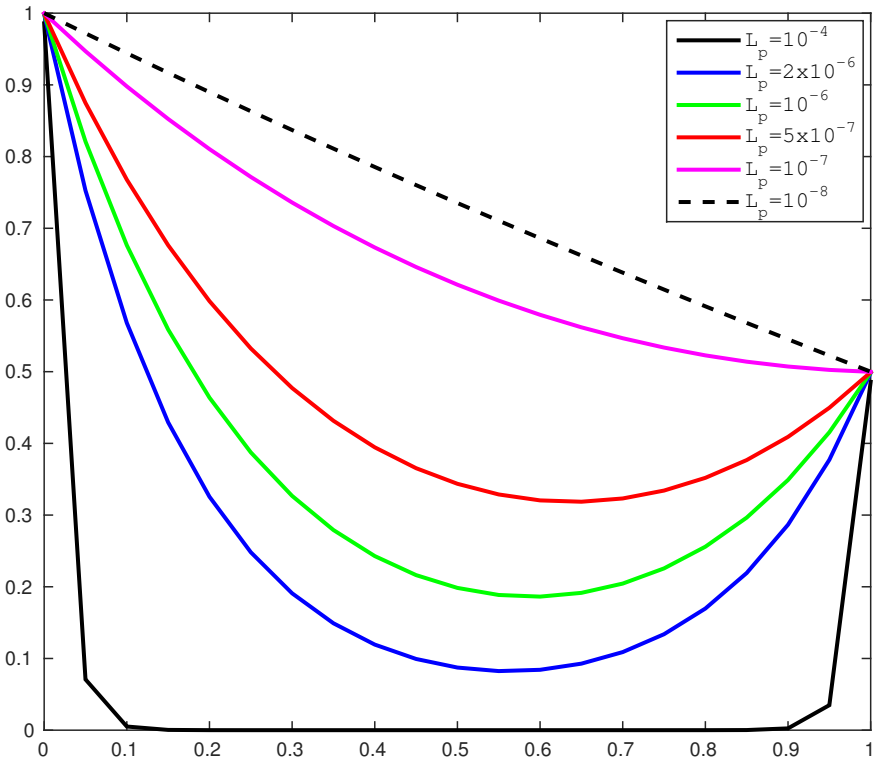

Fig. 5 Capillary pressure as function of arclength s for different vascular permeabilities $\hat{L}_p = 10^{-4}, 2\times10^{-6}, 10^{-6}, 5\times10^{-7}, 10^{-7}, 10^{-8}$. To be compared with Fig.7 in [5].

In addition, a sensitivity analysis has been performed to investigate the influence of the relative position of the 3D and 1D grids. To this purpose, we simulated three different configurations in which the network vertexes coincide with particular points of the 3D mesh, as shown in Figure 6. Numerical results of similar test cases, where the 1D mesh is slightly shifted to coincide with the location of Figure 6 (top), are given in Figure 6 (bottom). These results suggest that when the 1D mesh is not aligned with edges or faces of the 3D one, the velocity field in the neighborhood of the vessel looks smooth and symmetric. A similar conclusion holds true also when the 1D branch lays on the 3D mesh faces. However, a problematic case is observed when the 1D mesh entirely coincides with edges of the 3D one. In this case, the velocity field looses cylindrical symmetry around the 1D capillary. A preliminary and heuristic interpretation of this behavior can be found observing that the Raviart-Thomas degrees of freedom are located on the element faces. For this reason, the 3D velocity field is not uniquely defined on tetrahedral element edges. When the 1D source term is exactly located on the element edges, there is an inconsistency in the approximation of the velocity field.

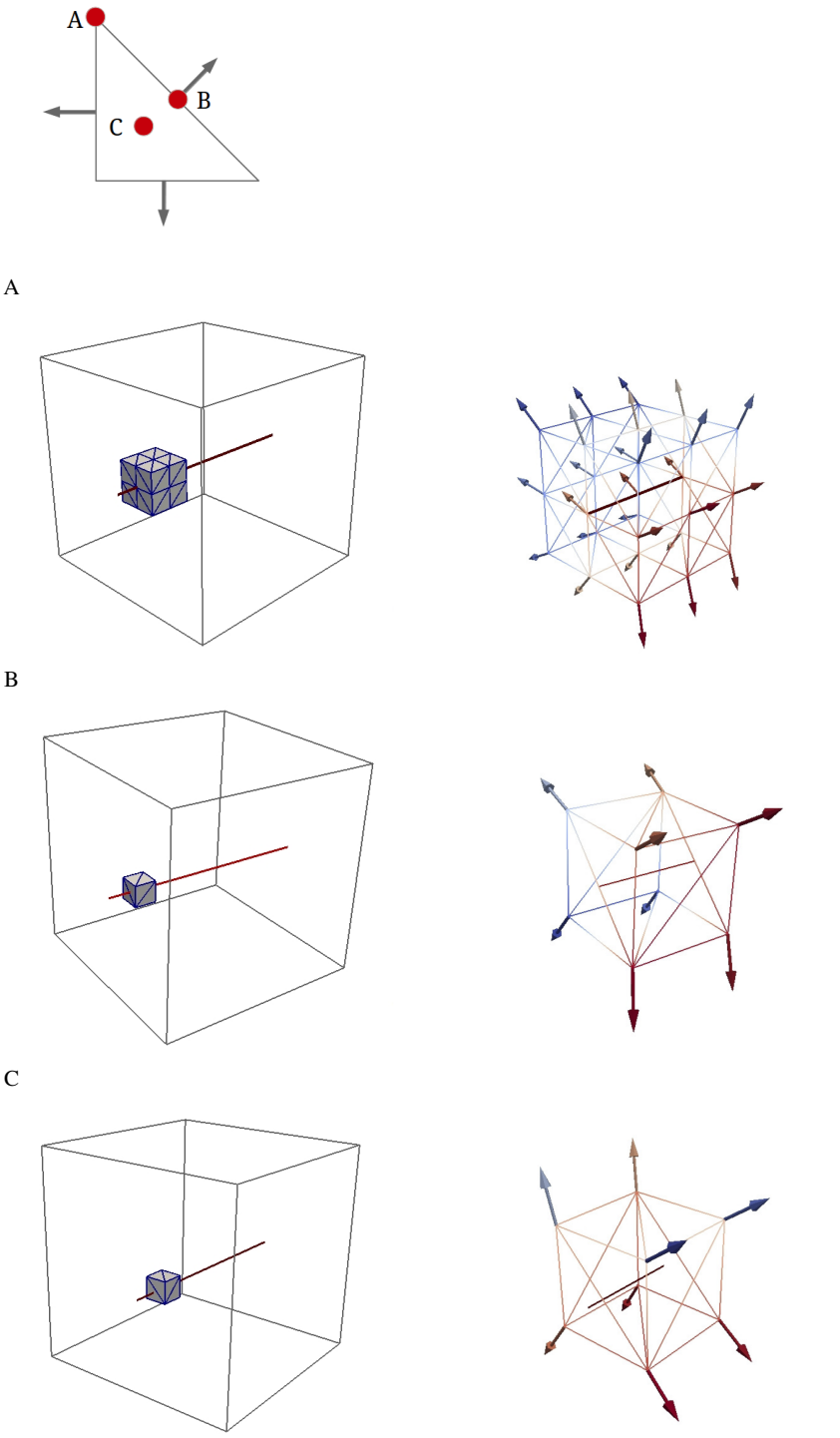

Fig. 6 (top panel) Proposed configurations for 1D/3D mesh correlation analysis. The red dots A, B, C indicate three meaningful configurations w.r.t. the distribution of Raviart-Thomas dof (arrows). We show below the sensitivity analysis for the 1D/3D mesh coupling. Numerical solutions have been obtained with mesh size $h = 0.1$ and parameters $\kappa_t = \kappa_v = 1$, $R' = 1$, $Q = 10^{-4}$. For each of the three configurations A, B, C, we extract the smallest patch of elements intersected by the 1D mesh (truncated along the axial direction for visualization purposes). The *local* velocity field is also displayed together with its magnitude (color scale).

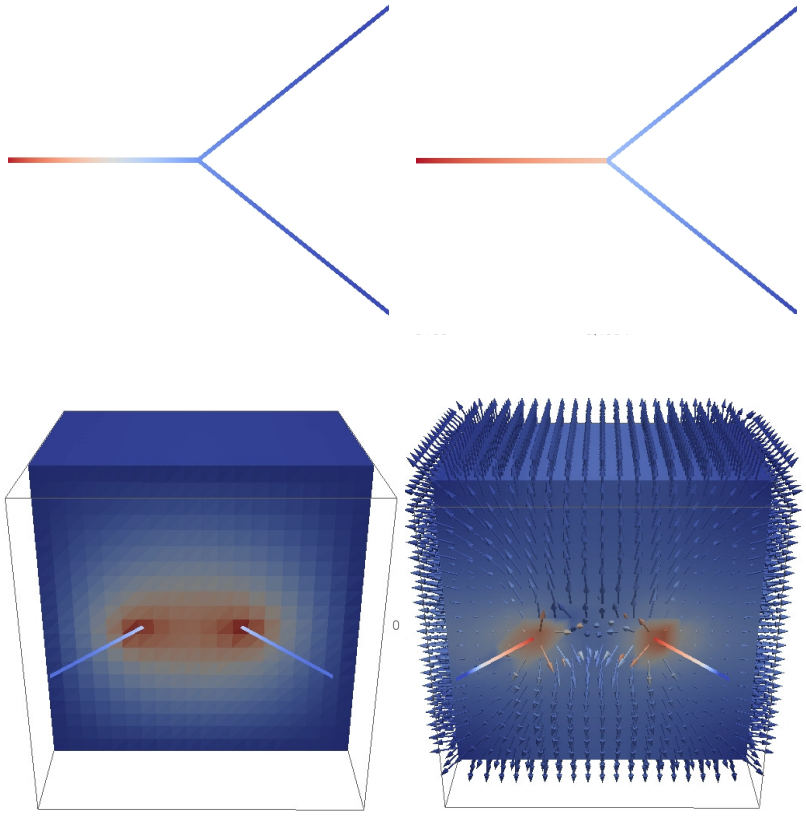

Fig. 7 (top) Numerical solution of the 1D vessel problem, $(p_{v,h}, u_{v,h})$ obtained with $h = 0.05$ and unitary parameters $\kappa_v = 1$, $R' = 1$, $Q = 1$. As expected the pressure (left) is almost linearly decreasing between the imposed boundary values 1 and 0; velocity (right) is almost constant over each branch and it halves after the junction. (bottom) Visualization of the 3D/1D coupled pressure and velocity fields.

5.2 Coupled 3D-1D problem on a Y-shaped bifurcation

We aim to validate the imposition of the mass conservation constraint at the junction. We observe that the conservation of total pressure at the junction $\mathbf{x}_M$,

$$p_v^0(\mathbf{x}_M) = p_v^1(\mathbf{x}_M) = p_v^2(\mathbf{x}_M) \equiv p_v(\mathbf{x}_M) \,, \tag{35}$$

is automatically ensured thanks to the use of continuous finite elements for the vessels pressure approximation. Conversely, in order to impose the mass conservation constraint

$$u_v^0(\mathbf{x}_M) = u_v^1(\mathbf{x}_M) + u_v^2(\mathbf{x}_M) \ , \tag{36}$$

we proceed as in (30). In practice, in the simple Y-shaped configuration, we first identify the FEM degrees of freedom (dofs) related to the same junction node. For those dofs we add in some specific entries of the problem matrix $+1$ for each inflow branch and -1 for each outflow branch.

5.2.1 Numerical results

We apply again the *SuperLU* direct method to solve the linear system (31) and boundary conditions as in the second test-case, (33).

We notice that both vessels pressure and velocity confirm the expected behavior along the network: the former is continuous everywhere while the latter is split into two after the junction. We then conclude that conditions (35) and (36) are fulfilled also at the numerical level. Furthermore, Fig.7 (bottom panel) confirms that, also in this case, the 3D/1D coupling behaves correctly.

Finally, we present in Figure 8 a comparison against the pressure formulation of the 3D/1D coupled problem (6), previously proposed in [3, 4]. In that work, only the p_t and p_v variables were approximated, in particular using piecewise linear finite elements. The velocity field was reconstructed a-posteriori, after calculating the pressure gradients as constant vector functions over each element. By comparing the results of the *new* mixed-form model (left column) against those of the pressure-form model (right column) it appears, as expected, that we lose accuracy in 3D pressure approximation, because we use piecewise constant approximation instead of piecewise linears, but we visibly gain a better approximation of the 3D velocity field. This is ultimately a very important advantage. Indeed, following the work of [3, 16] we are planning to combine these simulations with mass transport problems for drug delivery through the microcirculation, where the velocity field is adopted to model advection.

6 Conclusions

We have proposed a mixed finite element formulation for coupled incompressible flow problems defined on a 1D domain embedded into a 3D porous medium. Because of the non standard coupling operators based on nonlocal restriction of the 3D solution to the 1D manifold, the definition and implementation of the method is challenging. We have implemented a non-standard finite element method into a C++ solver and the purpose of this work was to carefully validate it on two benchmark problems. The numerical solutions feature the expected behavior and confirm the correct functioning of the code. The mixed finite element approximation for 3D/1D coupled incompressible flow problems is a significant improvement with respect to the previously available solver based on the primal pressure formulation, because

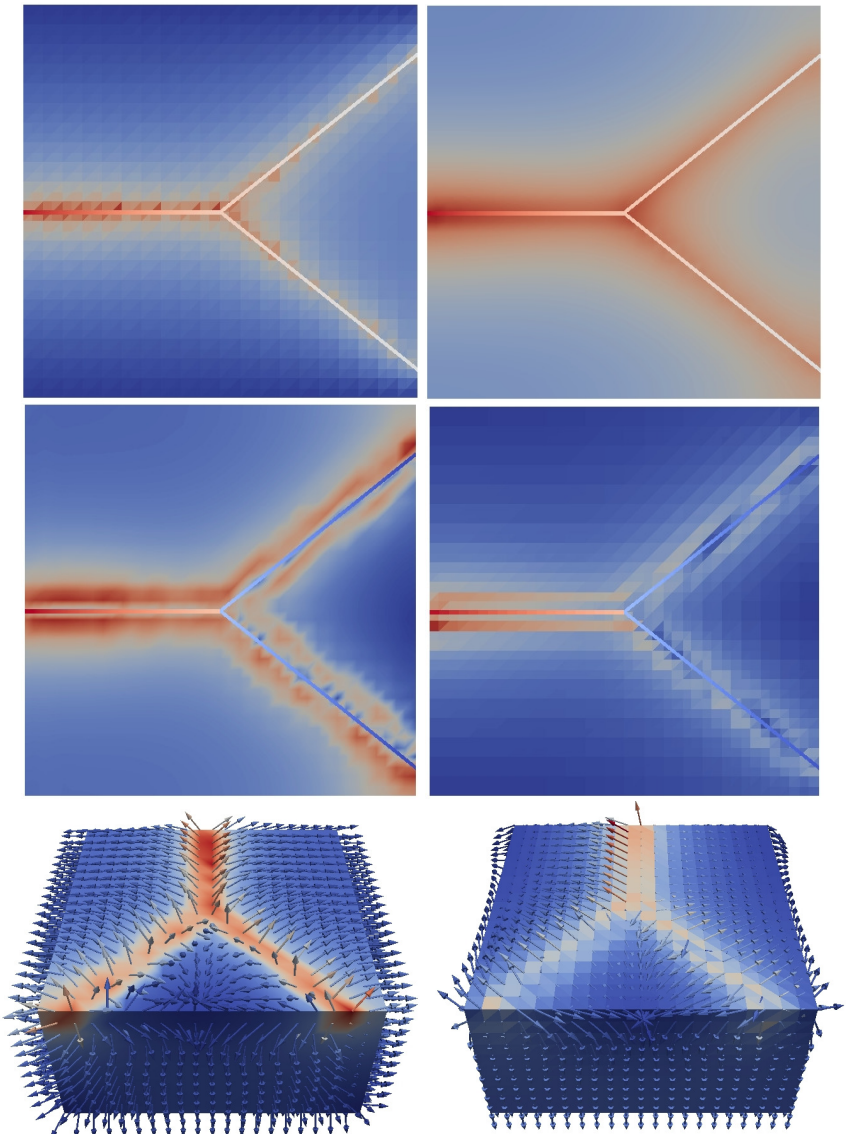

Fig. 8 Comparison between numerical predictions of pressure-form (right column) and mixed-form (left column) models within identical settings. In both cases we adopted $h = 0.05$ and dimensionless parameters $R' = 0.1$, $\kappa_t = 1$, $\kappa_v = 1$, $Q = 1$.

the velocity field is a variable of the problem and mass conservation constraints are directly enforced. Indeed, we are planning to exploit the better approximation properties of the velocity field, to combine the present solver with mass transport equations.

References

1. Blake, T., Gross, J.: Analysis of coupled intra- and extraluminal flows for single and multiple capillaries. Mathematical Biosciences **59**(2), 173–206 (1982)
2. Brezzi, F., Fortin, M.: Mixed and hybrid finite element methods, *Springer Series in Computational Mathematics*, vol. 15. Springer-Verlag, New York (1991). DOI 10.1007/978-1-4612-3172-1. URL http://dx.doi.org/10.1007/978-1-4612-3172-1
3. Cattaneo, L., Zunino, P.: A computational model of drug delivery through microcirculation to compare different tumor treatments. International Journal for Numerical Methods in Biomedical Engineering **30**(11), 1347–1371 (2014). DOI 10.1002/cnm.2661. URL http://dx.doi.org/10.1002/cnm.2661
4. Cattaneo, L., Zunino, P.: Computational models for fluid exchange between microcirculation and tissue interstitium. Networks and Heterogeneous Media **9**(1), 135–159 (2014)
5. Chapman, S.J., Shipley, R.J., Jawad, R.: Multiscale modeling of fluid transport in tumors. Bulletin of Mathematical Biology **70**(8), 2334–2357 (2008). DOI 10.1007/s11538-008-9349-7. URL http://dx.doi.org/10.1007/s11538-008-9349-7
6. D'Angelo, C.: Finite element approximation of elliptic problems with dirac measure terms in weighted spaces: Applications to one- and three-dimensional coupled problems. SIAM Journal on Numerical Analysis **50**(1), 194–215 (2012)
7. D'Angelo, C., Quarteroni, A.: On the coupling of 1d and 3d diffusion-reaction equations. application to tissue perfusion problems. Mathematical Models and Methods in Applied Sciences **18**(8), 1481–1504 (2008)
8. Fleischman, G., Secomb, T., Gross, J.: The interaction of extravascular pressure fields and fluid exchange in capillary networks. Mathematical Biosciences **82**(2), 141–151 (1986)
9. Flieschman, G., Secomb, T., Gross, J.: Effect of extravascular pressure gradients on capillary fluid exchange. Mathematical Biosciences **81**(2), 145–164 (1986)
10. Formaggia, L., Gerbeau, J., Nobile, F., Quarteroni, A.: On the coupling of 3d and 1d navier-stokes equations for flow problems in compliant vessels. Computer Methods in Applied Mechanics and Engineering **191**(6-7), 561–582 (2001). DOI 10.1016/S0045-7825(01)00302-4
11. Glowinski, R., Pan, T.W., Hesla, T., Joseph, D.: A distributed lagrange multiplier/fictitious domain method for particulate flows. International Journal of Multiphase Flow **25**(5), 755–794 (1999)
12. Glowinski, R., Pan, T.W., Periaux, J.: A fictitious domain method for dirichlet problem and applications. Computer Methods in Applied Mechanics and Engineering **111**(3-4), 283–303 (1994)
13. Hicks, K., Pruijn, F., Secomb, T., Hay, M., Hsu, R., Brown, J., Denny, W., Dewhirst, M., Wilson, W.: Use of three-dimensional tissue cultures to model extravascular transport and predict in vivo activity of hypoxia-targeted anticancer drugs. Journal of the National Cancer Institute **98**(16), 1118–1128 (2006)
14. Lesinigo, M., D'Angelo, C., Quarteroni, A.: A multiscale darcy-brinkman model for fluid flow in fractured porous media. Numerische Mathematik **117**(4), 717–752 (2011)
15. Mittal, R., Iaccarino, G.: Immersed boundary methods. Annual Review of Fluid Mechanics **37**, 239–261 (2005)
16. Nabil, M., Decuzzi, P., Zunino, P.: Modelling mass and heat transfer in nano-based cancer hyperthermia. Royal Society Open Science **2**(10) (2015). DOI 10.1098/rsos.150447. URL http://rsos.royalsocietypublishing.org/content/2/10/150447

17. Peskin, C.S.: The immersed boundary method. Acta Numer. **11**, 479–517 (2002). DOI 10.1017/S0962492902000077. URL http://dx.doi.org/10.1017/S0962492902000077
18. Quarteroni, A., Formaggia, L., Veneziani, A.: Cardiovascular mathematics: Modeling and simulation of the circulatory system. Modeling, Simulation and Applications **1**, 1–512 (2009)
19. Secomb, T., Hsu, R., Braun, R., Ross, J., Gross, J., Dewhirst, M.: Theoretical simulation of oxygen transport to tumors by three-dimensional networks of microvessels. Advances in Experimental Medicine and Biology **454**, 629–634 (1998)
20. Secomb, T., Hsu, R., Park, E., Dewhirst, M.: Green's function methods for analysis of oxygen delivery to tissue by microvascular networks. Annals of Biomedical Engineering **32**(11), 1519–1529 (2004)
21. Yu, Y., Baek, H., Karniadakis, G.: Generalized fictitious methods for fluid-structure interactions: Analysis and simulations. Journal of Computational Physics **245**, 317–346 (2013)
22. Zhang, L., Gerstenberger, A., Wang, X., Liu, W.K.: Immersed finite element method. Comput. Methods Appl. Mech. Engrg. **193**(21-22), 2051–2067 (2004). DOI 10.1016/j.cma.2003.12.044. URL http://dx.doi.org/10.1016/j.cma.2003.12.044

MOX Technical Reports, last issues

Dipartimento di Matematica
Politecnico di Milano, Via Bonardi 9 - 20133 Milano (Italy)

43/2016 Ambrosi, D.; Ciarletta, P.; De Falco, C.; Taffetani, M.; Zunino, P.
A multiscale modeling approach to transport of nano-constructs in biological tissues

42/2016 Iannetti, L.; D'Urso, G.; Conoscenti, G.; Cutri, E.; Tuan, R.S.; Raimondi, M.T.; Gottardi, R.; Zu
Distributed and lumped parameter models for the characterization of high throughput bioreactors

38/2016 Quarteroni, A.; Manzoni, A.; Vergara, C.
The Cardiovascular System: Mathematical Modeling, Numerical Algorithms, Clinical Applications

39/2016 Andrà, C.; Brunetto, D.; Parolini, N.; Verani, M.
Student interactions during class activities: a mathematical model

40/2016 Miglio, E.; Parolini, N.; Penati, M.; Porcù R.
High-order variational time integrators for particle dynamics

41/2016 Giovanardi, B.; Scotti, A.; Formaggia, L.
A hybrid XFEM - Phase Field (Xfield) method for crack propagation in brittle materials

37/2016 Tugnoli, M; Abbà, A. ; Bonaventura, L.; Restelli, M.
A locally p-adaptive approach for Large Eddy Simulation of compressible flows in a DG framework

36/2016 Mancini, L.; Paganoni, A.M.
Marked Point Process models for the admissions of heart failured patients

34/2016 Menafoglio, A.; Secchi, P.
Statistical analysis of complex and spatially dependent data: a review of Object Oriented Spatial Statistics

35/2016 Zonca, S.; Formaggia, L.; Vergara, C.
An unfitted formulation for the interaction of an incompressible fluid with a thick structure via an XFEM/DG approach